Future Cities and Environment
ISSN 2363-9075 Volume 11 (2025)

https://doi.org/10.70917/fce-2025-032
Article

Performance Analysis of Salt-In-Pumice Composites Under Varying Air Velocities for Thermochemical Heat Storage

Aslı Akyol Inada [1] and Devrim Aydin [1,2,*]

[1] Department of Mechanical Engineering, Eastern Mediterranean University, G. Magosa, TRNC Mersin 10, Türkiye
[2] Department of Architecture and Built Environment, The University of Nottingham, University Park, Nottingham, NG7 2RD, UK
* Corresponding author: devrim.aydin1@nottingham.ac.uk

Abstract: Thermochemical energy storage (TCES) offers significant potential for reducing reliance on fossil fuels while enhancing the utilization of renewable energy sources. The performance of TCES systems is critically influenced by the properties of thermochemical heat storage materials (TCMs), which directly affect both energy efficiency and storage capacity. In this study, a laboratory-scale experimental investigation was conducted to assess the performance of three pumice-based composite TCMs (P/LiCl-$CaCl_2$, P/$CaCl_2$, and CS-P/$CaCl_2$) under varying air velocities. Pumice particles with diameters of 1–3 mm were employed for P/LiCl-$CaCl_2$ and P/$CaCl_2$, whereas coarse size (CS) (4–6 mm) pumice was used for CS-P/$CaCl_2$. The primary objective was to evaluate the effects of particle size and LiCl incorporation on the thermal performance of composite TCMs. Key performance indicators, including energy efficiency (η_I), exergy efficiency (η_{II}), energy storage density (E_d), and outlet peak temperature ($T_{o,p}$), were determined. For P/LiCl-$CaCl_2$, average energy efficiencies of 64.0% and 76.6% were recorded at air velocities of 2.1 m/s and 3.7 m/s, respectively, with corresponding exergy efficiencies of 10.5% and 11.2%, and $T_{o,p}$ values of 46.4 °C and 47.7 °C. The P/$CaCl_2$ composite achieved lower performance, with energy efficiencies of 44.7% and 48.4%, exergy efficiencies of 4.9% and 5.2%, and $T_{o,p}$ values of 42.5 °C and 39.0 °C. For CS-P/$CaCl_2$, energy efficiencies were 64.2% and 72.2%, exergy efficiencies were 5.8% and 5.4%, and $T_{o,p}$ values were 40.9 °C and 39.0 °C, respectively. The maximum E_d of approximately 181 kWh/m³ was observed for P/LiCl-$CaCl_2$ at 3.7 m/s. Across all composite materials, both energy efficiency and E_d increased with higher air velocity. Furthermore, the exergy efficiency of P/LiCl-$CaCl_2$ was nearly double that of the other two composites, indicating a clear advantage of LiCl incorporation combined with smaller pumice particle sizes.

Keywords: thermochemical energy storage; composite sorbent; energy and exergy

1. Introduction

With the increase in global energy demand and growing environmental concerns, it has become imperative to use renewable energy resources more effectively and sustainably to reduce dependence on fossil fuels (Wang et al., 2025). Accordingly, energy storage technologies play a critical role in ensuring the balance between energy supply and demand (Inada, Rezaei and Aydin, 2025). Thermochemical energy storage (TCES) systems hold significant potential for long-term energy storage, owing to their high storage densities and minimal heat losses. (Padamurthy et al., 2025; Al Ghosini and Aydin, 2024). One of the basic components that directly affect the efficiency of TCES systems is thermochemical heat storage materials (TCMs) (Abdullah et al., 2024). In addition to the thermal and exergy performances of these materials, their energy storage densities are also important parameters that determine the overall success of the system. A suitable TCM should have high water vapor absorption capacity, low dehydration temperature, high cyclic stability and economic viability.

In the literature, salts such as calcium chloride ($CaCl_2$) (Karim Nejhad and Aydin, 2019) and lithium chloride (LiCl) (Yu et al., 2015) are frequently preferred due to their promising water retention properties and high heat storage capacities. When used directly, these salts often have disadvantages such as low heat transfer coefficient and structural stability (e.g., deliquescence) issues. Microscopic particle agglomerates, particularly those formed by the dissolution of salts, can block the heat transfer channels between the reactor and the energy storage material, reducing efficiency (Zhang et al., 2024). To overcome these problems, compositing with porous host matrices improves both heat transfer performance and structural stability. In such composite TCMs, the pore structure, particle size, and distribution of the TCM directly affect moisture diffusion and heat transfer, determining charging and discharging efficiency (Zhang et al., 2025; Wei et al., 2022). Recent studies investigated a wide range of salt-in-matrix composite TCMs in different TCES configurations. The study by Hu et al. (2025) demonstrated that $SrCl_2$/$CaCl_2$ binary hydrated salt composites supported on expanded perlite exhibit improved hydration kinetics and thermal storage performance compared to mono-salt composites. The optimal $SrCl_2$ to $CaCl_2$ ratio of 2:1 with 30% salt impregnation achieved a high adsorption capacity and heat storage density, alongside enhanced cycling stability, reducing issues such as deliquescence and structural damage. Zhang et al. (2025) developed and experimentally validated two TCES configurations integrating with domestic water heating systems. The detached finned microchannel heat exchanger (DFHEX-TCES) outperformed the internal bare microchannel heat exchanger (IBHEX-TCES) by maintaining higher temperature lifts for longer durations, particularly under increased airflow and multilayer designs, demonstrating promising applicability for residential water heating with enhanced thermal performance. Wei et al. (2024) investigated a two-stage adsorption mechanism in $SrCl_2$-metal-organic framework (MOF) composites, revealing that $SrCl_2$ acts as a moisture pump to enhance water vapor capture, while MOFs serve as water reservoirs. The SrCl2@MIL-101(Cr) composite achieved superior water sorption capacity (0.825 g/g) and heat storage enthalpy (1462 kJ/kg) with reduced dehydration temperature, providing insights for designing advanced porous TCMs. Farcot et al. (2019) studied a moving-bed thermochemical reactor using $SrBr_2$ hydrate salts for building heating, achieving reactor temperatures up to 41 °C and heating power densities of up to 4.6 kW/m³. The work highlighted the impact of inlet air humidity on reactor performance and demonstrated the feasibility of continuous TCES with moving-bed reactors. Li et al. (2025) synthesized a novel LiCl@Al-Fum-Al_2O_3 TCM enhanced with nano-Al_2O_3 to improve thermal conductivity and adsorption performance. The composite exhibited an 85% increase in heat of adsorption and stable cycling behavior over 20 cycles, indicating significant potential for improving efficiency and stability in TCES systems using aluminum-based MOF adsorbents. John et al. (2024) performed experimental and numerical analyses of a packed-bed thermochemical energy storage system using K_2CO_3 salt. They identified optimal operating conditions, including a mass flow rate of 0.03 kg/s and inlet temperature of 80 °C, which maximized reaction advancement and temperature output. The study validated a 3D transient model correlating well with experiments, aiding in optimizing charging and discharging processes. Hao et al. (2024) proposed a multi-module columnar packed-bed reactor for salt hydrate thermochemical heat storage, comparing top peripheral and bottom central air intake designs. The bottom central intake scheme yielded more uniform reactions, shorter times, and higher efficiency. Increasing inlet air temperature and velocity further improved performance, offering valuable design guidance for enhancing TCES reactors. Liu et al. (2024) explored fluidised-bed TCES using composite salts in porous matrices (CSPMs) suitable for low-temperature applications. The $CaCl_2$/mesoporous silica composite exhibited the best heat discharge performance, with high energy storage density and fluidization stability over cycles. This work advances the potential for fluidised-bed systems in low-grade heat storage.

Barbosa and Menon (2024) addressed material instability issues in $SrCl_2$ and $MgCl_2$ salts by fabricating binary mixtures with reduced particle size, improving hydration kinetics and structural stability. The 50/50 $SrCl_2$-$MgCl_2$ mixture extended hydration reaction conditions and achieved a high specific energy density and thermal power output, offering a standardized approach for designing stable, high-performance thermochemical salt mixtures.

In the literature, several different composites have been investigated for TCES applications. However, only a few studies have explored pumice-based composites (Al Ghosini and Aydin, 2024; Mehrabadi and Farid, 2018). Therefore, the present study aims to develop and experimentally evaluate salt-in-pumice composites under different operating conditions to assess their potential as efficient and durable TCMs. Pumice is highly suitable as a porous host matrix for TCES due to its low density, high porosity, and excellent thermal stability (Al Ghosini and Aydin, 2024; Aarts et al., 2025). Its natural porous structure provides a large surface area that facilitates efficient salt impregnation and vapor diffusion, enhancing hydration and dehydration kinetics. Additionally, pumice's chemical inertness and mechanical strength ensure durability and long-term cycling stability in TCES applications. Within the study, three different salt-in pumice composites were investigated: P/LiCl-$CaCl_2$ (using 1-3 mm diameter pumice),

P/$CaCl_2$ (using 1-3 mm dimeter pumice) and P/$CaCl_2$ (using coarse pumice with a 4-6 mm dimeter). The performance of the synthesised TCMs was experimentally evaluated under laboratory conditions at varying air velocities. The energy and exergy efficiencies of the materials, energy storage densities and outlet temperatures were compared. The findings reveal that the performances of TCMs vary depending on the air velocity and material composition and emphasize the importance of material selection and optimisation of the operating conditions for TCES systems.

2. Materials and Methods

2.1. Synthesis of Composite Thermochemical Materials (TCMs)

In this study, three different TCMs were synthesised as P/LiCl-$CaCl_2$, P/$CaCl_2$ and CS-P/$CaCl_2$. The P/LiCl–$CaCl_2$ composite was prepared by mixing LiCl and $CaCl_2$ salts in equal mass proportions (50:50) and incorporating pumice with a particle size of 1–3 mm as the host matrix. On the other hand, two different P–$CaCl_2$ composites were prepared: one using pumice particles with a diameter of 1–3 mm, and the other using coarse pumice particles with a diameter of 4–6 mm. The TCM containing 1–3 mm pumice is referred to as P–$CaCl_2$, while the TCM containing 4–6 mm pumice is designated as CS–P/$CaCl_2$. By developing three different composites with single and binary salt mixtures and varying host matrix particle sizes, this study aims to investigate the effects of pumice particle size and the presence of LiCl on TCM performance.

2.2. Experimental Setup and Test Procedure

The TCES system used in this study is designed to comparatively investigate different TCM performances under different inlet air conditions. The experimental setup is presented in Figure 1. The system consists of a fixed-bed TCES reactor integrated into an air conditioning unit. The air conditioning unit is equipped with a variable-speed radial fan and four electric heating elements (two 1 kW and two 0.5 kW) for use in the charging cycle. In the discharging cycle, an external ultrasonic humidifier is integrated into the air conditioning unit inlet to increase the relative humidity of the inlet air. The TCES reactor located at the outlet of the air conditioning unit is the main heat storage element of the system and these two units are configured to operate in an integrated manner. The TCES reactor is a rectangular box with dimensions of 370 mm × 330 mm × 460 mm and is insulated with 40 mm thick foil-coated glass wool. Inside the reactor, there is a wire mesh tray with dimensions of 350 mm × 310 mm × 32 mm, placed perpendicular to the air flow direction. This tray was used to place the TCM. The TCM was spread inside the tray in direct contact with the air flow. The air flow rate was controlled by a separate radial fan placed at the reactor outlet. During the performed discharging and charging experiments, sensirion SHTC3 sensors were used to measure the following parameters: Ambient temperature, inlet air temperature, inlet air humidity, outlet air temperature, and outlet air humidity. The sensors' temperature and humidity measurement ranges were 0-130 °C and 0-100 %, respectively, with accuracies of ±0.2°C and ±2%. The Pasco-Xplorer Anemometer was used to measure air velocity with an accuracy of ±0.1 m/s. The experimental results were subject to uncertainties arising from the combined measurement errors of the sensors, which depend on their specified accuracies, as detailed in Section 2.5. In addition, fluctuations in ambient temperature and humidity conditions within the laboratory during the testing period contributed to variability in the measurements. These environmental variations introduced further deviations that may have influenced the system’s performance and data consistency.

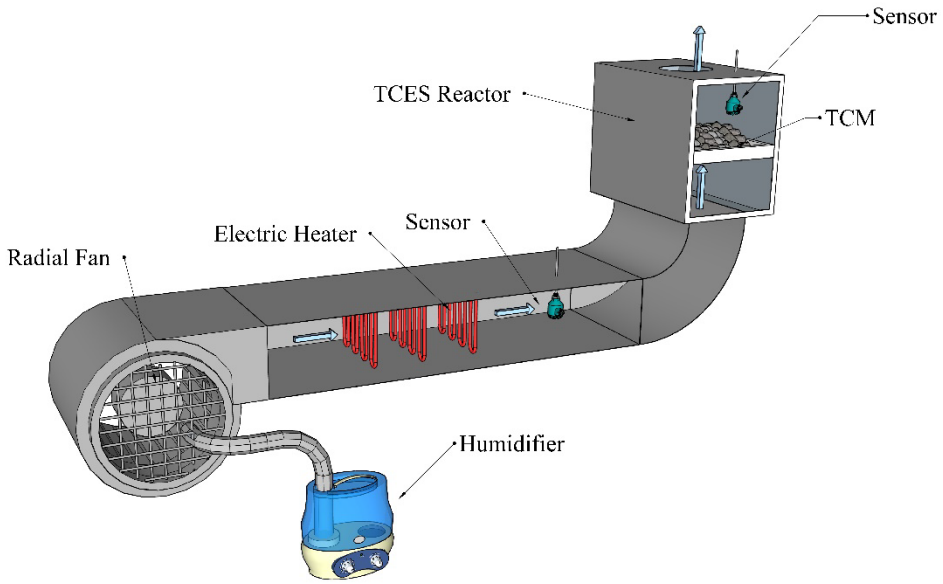

Figure 1. Schematic illustration of the experimental setup.

2.3. Methodology

In this study, the performances of three composite TCMs, P/LiCl-$CaCl_2$, P/$CaCl_2$ and CS-P/$CaCl_2$, were comparatively evaluated under different air velocities. In the experimental study, the discharging process was carried out for 60 minutes at T_{in} = 22–26°C and RH_{in} = 60–75%. The inlet air conditions were maintained consistently across tests with the help of adjustable ultrasonic humidifiers and the air conditioning unit equipped with electric heaters as described in Section 2.2. Charging cycles were carried out for 90 minutes at T_{in} = 60–80 °C. Tests were conducted at air velocities of 2.1 m/s and 3.7 m/s. Temperature and relative humidity changes were recorded every 30 seconds during the tests. Based on the obtained data, the heat transfer rates, cumulative energy and exergy values, energetic and exergetic efficiencies, and energy storage densities were calculated. Additionally, mass measurements were made before and after the experiments to determine the moisture absorption and desorption performances of TCMs.

2.4. Governing equations

The heat gain ($\dot{Q}_o$) of the air during the discharging process and heat supplied to the TCM ($\dot{Q}_i$) during the charging process are calculated by Equations (1) and (2):

$$\dot{Q}_o = \dot{m}_{dc} . c_p . (T_{o,dc-} T_{i,dc}) \quad (1)$$

$$\dot{Q}_i = \dot{m}_{chr} . c_p . (T_{i,chr-} T_{o,chr}) \quad (2)$$

where, $T_{o,dc}$ and $T_{i,dc}$ are the outlet and inlet temperature of the air during the discharging process, $T_{i,chr}$ and $T_{o,chr}$ are the inlet and outlet temperature of the air during the charging process, $\dot{m}_{dc}$ and $\dot{m}_{chr}$ are the mass flow rate of the air during the discharging and charging processes and c_p is the specific heat of air at constant pressure.

The exergy output ($\dot{E}x_o$) and input ($\dot{E}x_i$) during the discharging and charging processes are calculated with the Equations (3) and (4), respectively.

$$\dot{E}x_o = \dot{m}_{dc} . c_p \left[(T_{o,dc} - T_{i,dc}) - T_a \, ln \left(\frac{T_{o,dc}}{T_{i,dc}} \right) \right] \quad (3)$$

$$\dot{E}x_i = \dot{m}_{chr} . c_p . \left[(T_{i,chr} - T_{o,chr}) - T_a \, ln \left(\frac{T_{i,chr}}{T_{o,chr}} \right) \right] \quad (4)$$

The cumulative amount of heat gain during the discharging process and cumulative amount of heat supplied to the sorbent during the charging process can be calculated using the following Equations:

$$E_{cu,dc} = \dot{Q}_{o,ave} \cdot t_{dc} \quad (5)$$

$$E_{cu,chr} = \dot{Q}_{i,ave} \cdot t_{chr} \quad (6)$$

The cumulative exergy gain ($Ex_{cu,dc}$) and cumulative exergy supplied to the TCM ($Ex_{cu,chr}$) during the discharging and charging processes could be obtained in a similar way with Equations 5-6, by multiplication of the process durations with the $\dot{E}x_{out}$ and $\dot{E}x_{in}$ given in Equations 3-4.

The energy storage density (E_d) of the TCM is calculated by dividing the cumulative heat gain ($E_{cu,dc}$) obtained during the discharging phase by the volume of the TCM used (V_{TCM}):

$$E_d = \frac{E_{cu,dc}}{V_{TCM}} \quad (7)$$

The cyclic energetic efficiency (η_I) and exergetic efficiency (η_{II}) of the TCES unit are defined as the ratio of the cumulative energy or exergy released during the discharging cycle to the cumulative energy or exergy supplied to the TCM during the corresponding charging cycle:

$$\eta_I = \frac{E_{cu,dc}}{E_{cu,chr}} \quad (8)$$

$$\eta_{II} = \frac{Ex_{cu,dc}}{Ex_{cu,chr}} \quad (9)$$

2.5 Uncertainty Analysis

The percentage errors of the experimental results were obtained with uncertainty analysis. The uncertainty of the independent variables, w_Z, is represented by the variables w_1, w_2, w_3, …, w_n (Buker, Mempouo and Riffat, 2014).

$$w_Z = \left[\left(\frac{\partial R}{\partial y_1} w_1\right)^2 + \left(\frac{\partial R}{\partial y_2} w_2\right)^2 + \left(\frac{\partial R}{\partial y_3} w_3\right)^2 + \ldots + \left(\frac{\partial R}{\partial y_4} w_4\right)^2\right]^{1/2} \quad (10)$$

The total uncertainty of first law efficiency (η_I) as a function of $T_{o,dc}$, $T_{i,dc}$, $T_{o,chr}$, $T_{i,chr}$, V_{dc} and V_{chr} can be determined as follows;

$$w_Z = \left[\left(\frac{\partial \eta_I}{\partial T_{i,chr}} w_{T_{i,chr}}\right)^2 + \left(\frac{\partial \eta_I}{\partial T_{o,chr}} w_{T_{o,chr}}\right)^2 + \left(\frac{\partial \eta_I}{\partial T_{i,dc}} w_{T_{i,dc}}\right)^2 + \left(\frac{\partial \eta_I}{\partial T_{o,dc}} w_{T_{o,dc}}\right)^2 + \left(\frac{\partial \eta_I}{\partial V_{chr}} w_{V_{chr}}\right)^2 + \left(\frac{\partial \eta_I}{\partial V_{dc}} w_{V_{dc}}\right)^2\right]^{1/2} \quad (11)$$

Based on the Equation 11, the total uncertainty of η_I is obtained as 5.37%.

3. Result and Discussion

3.1. Discharging Analysis

Figures 2 and 3 show the variations in temperature and humidity for P/LiCl–$CaCl_2$ at air velocities of 2.1 m/s and 3.7 m/s, respectively. Similarly, Figures 4 and 5 present the variations for the P/$CaCl_2$, while Figures 6 and 7 illustrate those for the CS-P/$CaCl_2$ under the same respective air velocities. Inlet air temperatures and inlet humidity values were in the range of T_{in} = 22–26 °C and RH_{in} = 60–75%. The selected range for inlet air temperature and relative humidity was determined based on two primary considerations: the typical ambient conditions in moderate climate regions, and the operational boundaries of the experimental setup. These conditions are representative of real-world environments where TCES systems are intended to be deployed, particularly for building climate control or waste heat recovery applications. Relative humidity (RH) plays a significant role in the performance of TCES systems, especially during the adsorption phase. Higher RH levels increase the water vapor content in the inlet air, which enhances the adsorption potential of the sorbent material and leads to a more pronounced exothermic reaction, thus improving heat release. In contrast, lower RH conditions can limit the reaction rate and reduce thermal output. Therefore, maintaining an appropriate humidity level is critical to maximizing system efficiency. In this study, the chosen RH range allowed for observable variations in system behavior, aiding the analysis of performance sensitivity to ambient moisture conditions.

According to the testing results, the peak outlet temperature ($T_{o,p}$) of the P/LiCl–$CaCl_2$ was 46.4 °C at an air velocity of 2.1 m/s and 47.7 °C at 3.7 m/s (Fig. 2(a) and Fig 3(a)). The P/$CaCl_2$ exhibited $T_{o,p}$ values of 42.5 °C and 39.0 °C under the same respective air velocities (Fig. 4(a) and Fig 5(a)). For the CS-P/$CaCl_2$, $T_{o,p}$ values were 40.9 °C and 39.0 °C at 2.1 m/s and 3.7 m/s, respectively (Fig. 6(a) and Fig 7(a)). When comparing P–$CaCl_2$ and CS-P/$CaCl_2$, their performances were similar at the lower air velocity of 2.1 m/s. However, as the air velocity increased, P–$CaCl_2$ exhibited a more stable outlet temperature, indicating more promising discharging performance. This improvement is attributed to smaller particle size of P-$CaCl_2$ enabling larger TCM surface, which enhances heat and mass transfer. While high surface area offers little advantage at low air velocities, where the air–material contact time is already sufficient, it becomes a critical factor at higher velocities, where contact time is limited.

During the discharging cycle of P/LiCl-$CaCl_2$, the relative humidity of the outlet air dropped to nearly 10%, while the outlet temperature reached to a peak of nearly 47 °C at the beginning of the experiments with air velocities of 2.1 m/s and 3.7 m/s. In the following period, outlet relative humidity (Fig. 2 and Fig. 3) gradually increased to nearly 40% (v=2.1 m/s) and 47% (v=3.7 m/s). Meanwhile, due to the reduced sorption rate over the discharging duration, outlet temperature dropped to 28-29 °C. For P-$CaCl_2$ outlet relative humidity of air varied between 10-30% (Fig. 4b and Fig. 5b), while for CS-P/$CaCl_2$ it reached to far higher levels of 52% (v=2.1 m/s) and 60% (v=3.7 m/s) (Fig. 6b and Fig. 7b).

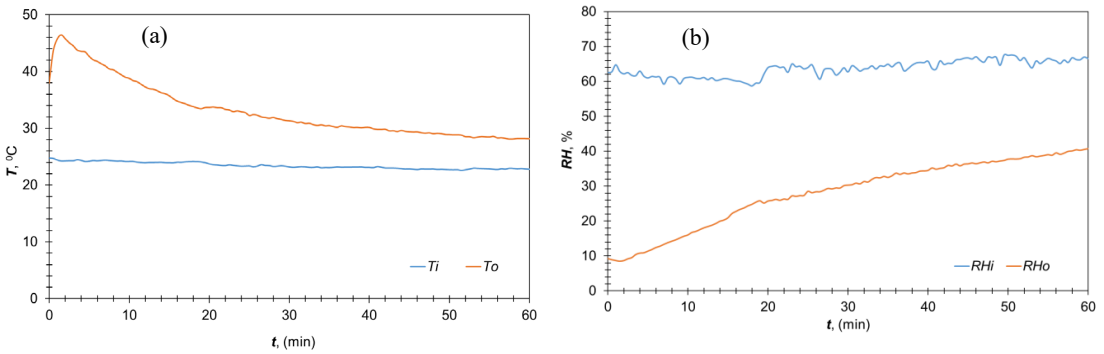

Figure 2. (a) Temperature and (b) humidity variations during the discharging process of P/LiCl-$CaCl_2$ at 2.1 m/s air velocity

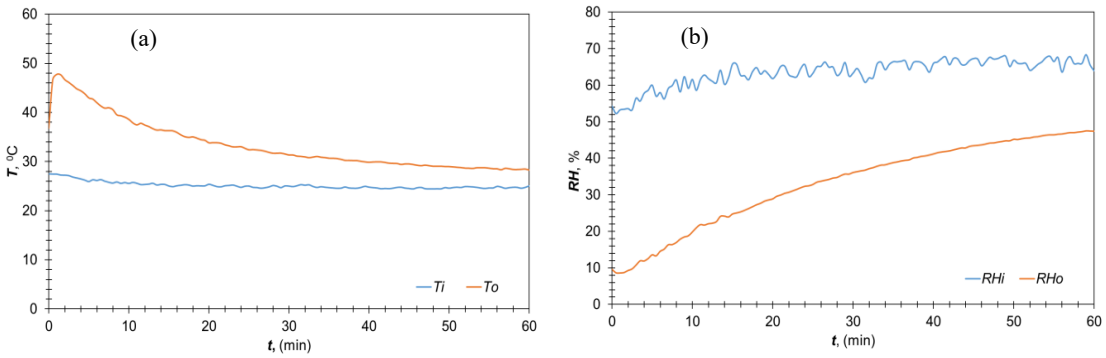

Figure 3. (a) Temperature and (b) humidity variations during the discharging process of P/LiCl-$CaCl_2$ at 3.7 m/s air velocity

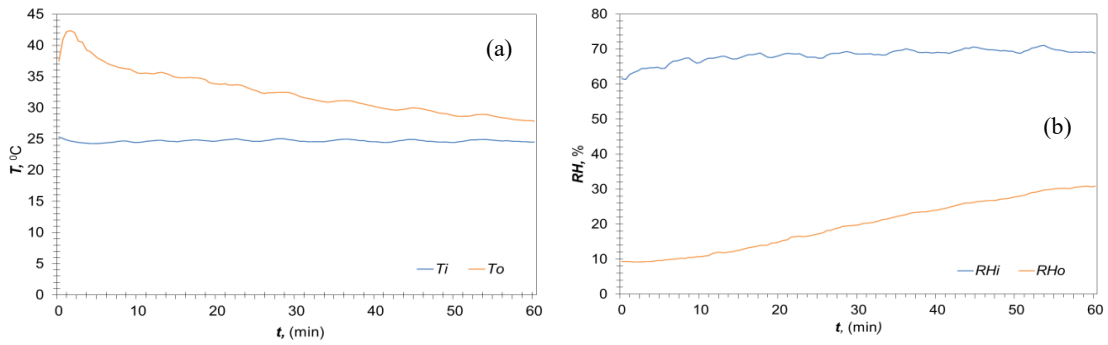

Figure 4. (a) Temperature and (b) humidity variations during the discharging process of P/$CaCl_2$ at 2.1 m/s air velocity

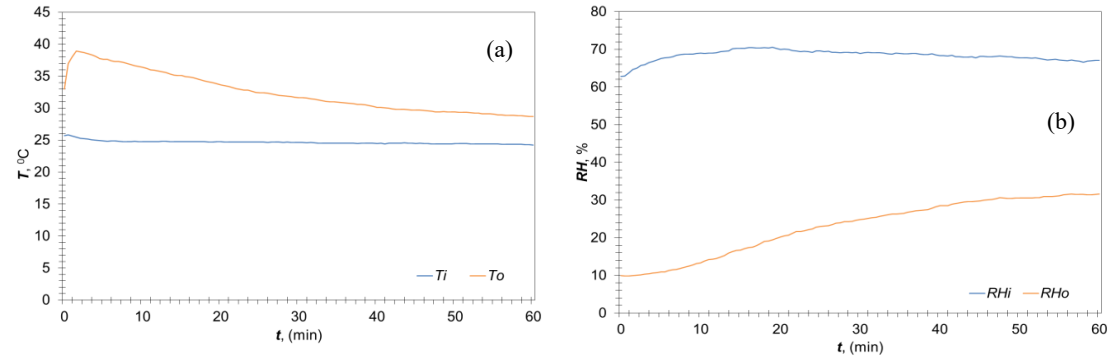

Figure 5. (a) Temperature and (b) humidity variations during the discharging process of P/$CaCl_2$ at 3.7 m/s air velocity

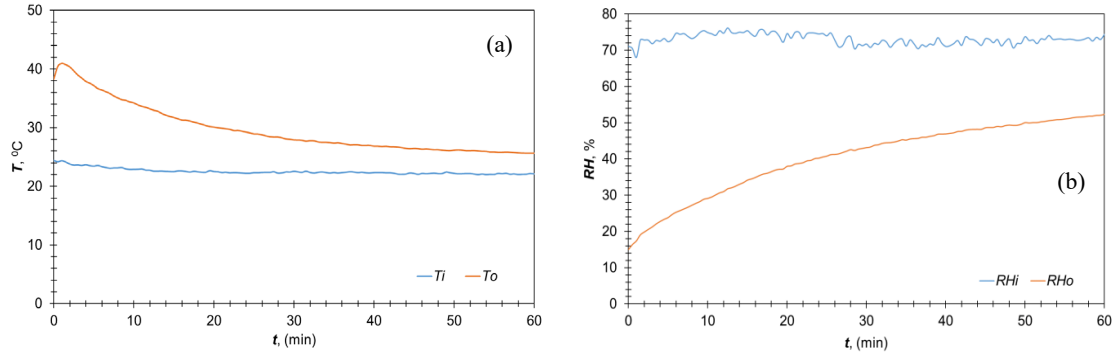

Figure 6. Temperature and (b) humidity variations during the discharging process of CS-P/$CaCl_2$ at 2.1 m/s air velocity

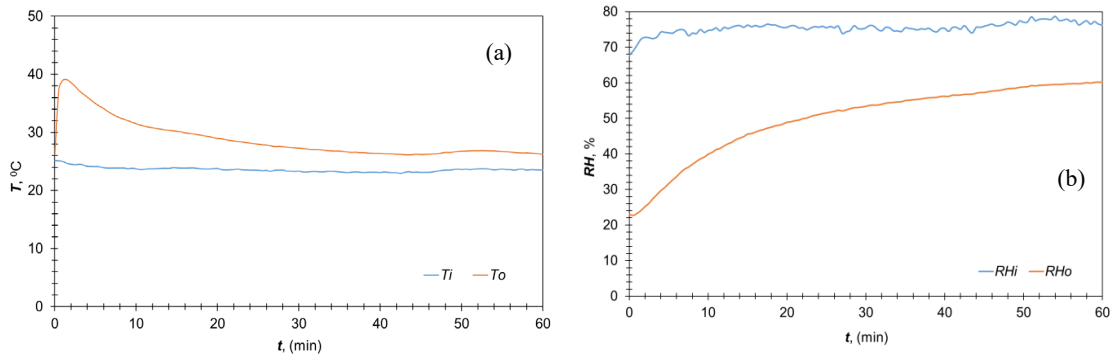

Figure 7. (a) Temperature and (b) humidity variations during the discharging process of CS-P/$CaCl_2$ at 3.7 m/s air velocity

Figure 8(a) and Figure 8(b) show the $\dot{Q}_o$ and E_d values for the tested TCMs at different air velocities, respectively. The $\dot{Q}_o$ of P/LiCl–$CaCl_2$ was 0.43 kW at an air velocity of 2.1 m/s and 0.63 kW at 3.7 m/s. For P/$CaCl_2$, the corresponding values were 0.34 kW and 0.60 kW, while CS-P/$CaCl_2$ achieved 0.32 kW and 0.40 kW, respectively. At an air velocity of 2.1 m/s, the highest E_d was recorded for P/LiCl–$CaCl_2$ (121.8 kWh/m³), followed by P/$CaCl_2$ (98.0 kWh/m³) and CS-P/$CaCl_2$ (90.75 kWh/m³). At 3.7 m/s, P/LiCl–$CaCl_2$ again achieved the highest value (181.3 kWh/m³), with P/$CaCl_2$ (170.5 kWh/m³) ranking second and CS-P/$CaCl_2$ (115.2 kWh/m³) third.

These results demonstrate that increasing air velocity significantly enhances the rate of heat release for all materials. Higher air velocity accelerates convective heat and mass transfer across the sorption bed, increasing the reactor heat output. It should be noted that the discharging experiments were limited to 60 minutes for the purpose of material comparison. Over longer durations, where the full stored heat is extracted, the influence of air velocity may differ. Therefore, extended tests across a wider range of velocities are recommended to determine the optimal operating conditions for TCES units.

The comparative results demonstrate that P/LiCl–$CaCl_2$ delivers the highest performance, followed by P/$CaCl_2$ and CS-P/$CaCl_2$ (CS-P/$CaCl_2$ < P/$CaCl_2$ < P/LiCl–$CaCl_2$) in terms of E_d and $\dot{Q}_o$. This superior performance of P/LiCl–$CaCl_2$ can be attributed to the synergistic effect of LiCl, which enhances moisture absorption and heat release during discharging. Additionally, the use of smaller-sized pumice in P/$CaCl_2$ contributes to more effective heat and mass transfer compared to coarse-sized pumice, explaining its advantage over CS-P/$CaCl_2$.

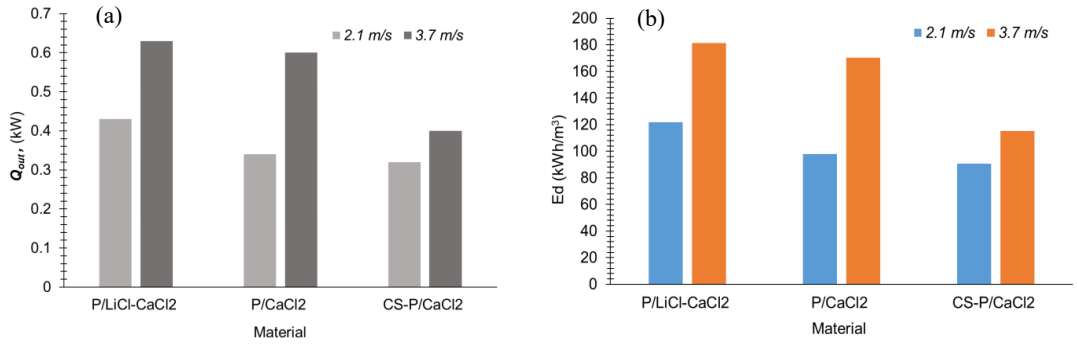

Figure 8. Effect of different air velocities on (a) heat output rate (b) energy storage density.

3.2. Charging Analysis

The thermal behaviors of the P/LiCl–$CaCl_2$, P/$CaCl_2$ and CS-P/$CaCl_2$ composite TCMs during charging at different air velocities are detailed in Figures 9 to 14. Figures 9(a) and 9(b) depict the air outlet temperature and relative humidity variations during the charging cycle of the P/LiCl–$CaCl_2$ composite at an air velocity of 2.1 m/s, while Figures 10(a) and 10(b) present the corresponding data at 3.7 m/s. For P/$CaCl_2$, the charging cycle results at 2.1 m/s and 3.7 m/s are shown in Figures 11 and 12, respectively. The CS-P/$CaCl_2$ composite results are illustrated in Figures 13(a) and 13(b) for 2.1 m/s and

Figures 14(a) and 14(b) for 3.7 m/s.

Throughout the charging cycle, the air inlet temperature varied between 60–80°C, depending on ambient conditions. Temperatures measured at the reactor outlet were between 30-40 °C initially. The outlet temperatures increased gradually as the desorption rate decreased and reached to a steady condition after 40-50 minutes following the start of the experiments. The observed outlet temperature profiles varied depending on the intensity of the endothermic reactions occurring within the TCMs and the air velocity. The decrease in the inlet-outlet temperature difference during the charging cycle indicates that water vapor desorption has ceased as the material's moisture content decreases, thus weakening the reaction rate. In this context, the P/LiCl–$CaCl_2$ composite exhibited a temperature difference of 10.1 °C at 2.1 m/s and 7.0 °C at 3.7 m/s. The decrease in temperature difference at higher air speeds suggests that the material dried faster and completed the charging process more efficiently. The P/$CaCl_2$ composite maintained a high temperature difference at both velocities (13.7 °C and 12.4 °C), indicating that complete moisture removal took longer and that the drying process progressed more slowly. The CS-P/$CaCl_2$ exhibits rapid drying potential with relatively low temperature differences (7.1 °C at 2.1 m/s and 4.7 °C at 3.7 m/s). This rapid discharging is partly due to its lower moisture retention capacity, meaning less moisture is held within the material and thus can be released more quickly. However, the larger pumice size results in wider air channels, which allows air to pass through the bed more easily. While this reduces pressure loss, it also decreases the contact time and surface area available for moisture transfer between the air and the sorbent material, thereby limiting moisture removal effectiveness compared to P/LiCl–$CaCl_2$ and P–$CaCl_2$. These observations reveal the significant effects of the air velocity and material structure used during the charging process on system performance. Increasing the air velocity increases heat transfer, resulting in more effective desorption, which contributes to the overall energy recovery efficiency of the system.

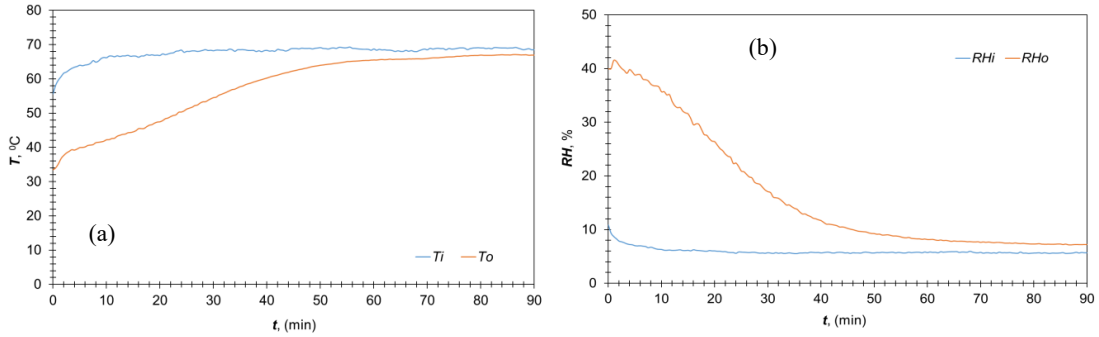

Figure 9. (a) Temperature and (b) humidity variations during the charging process of P/LiCl-$CaCl_2$ at 2.1 m/s air velocity.

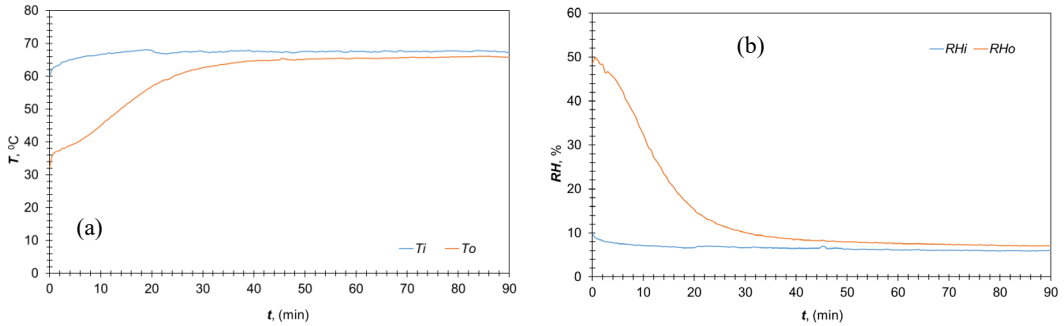

Figure 10. (a) Temperature and (b) humidity variations during the charging process of P/LiCl-$CaCl_2$ at 3.7 m/s air velocity.

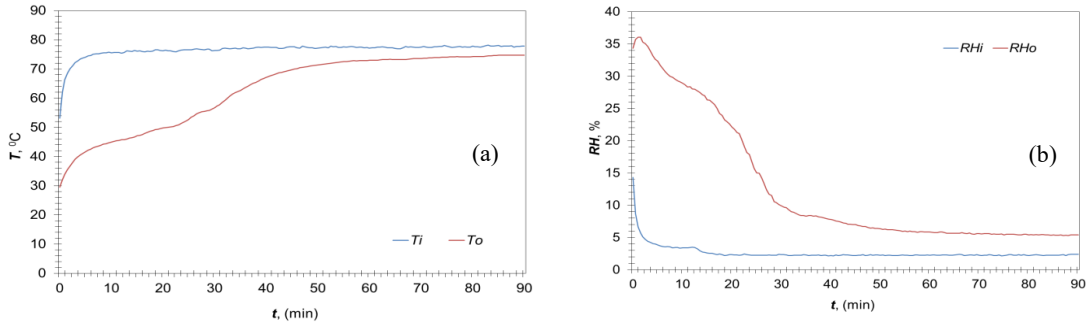

Figure 11. (a) Temperature and (b) humidity variations during the charging process of P/$CaCl_2$ at 2.1 m/s air velocity.

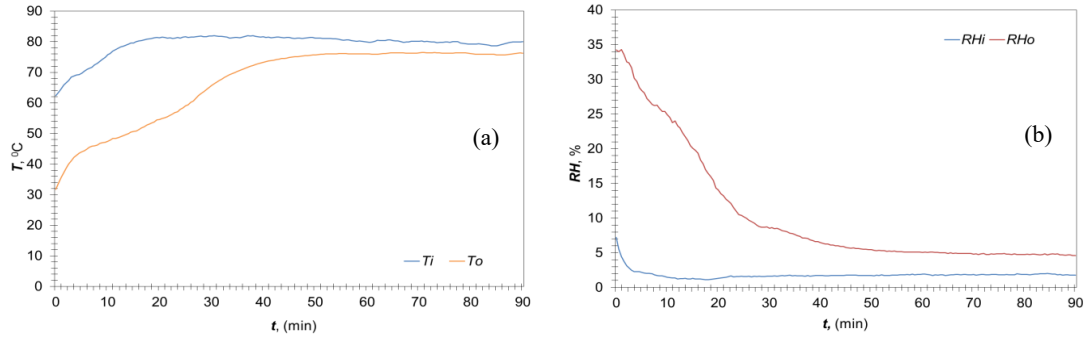

Figure 12. (a) Temperature and (b) humidity variations during the charging process of P/$CaCl_2$ at 3.7 m/s air velocity.

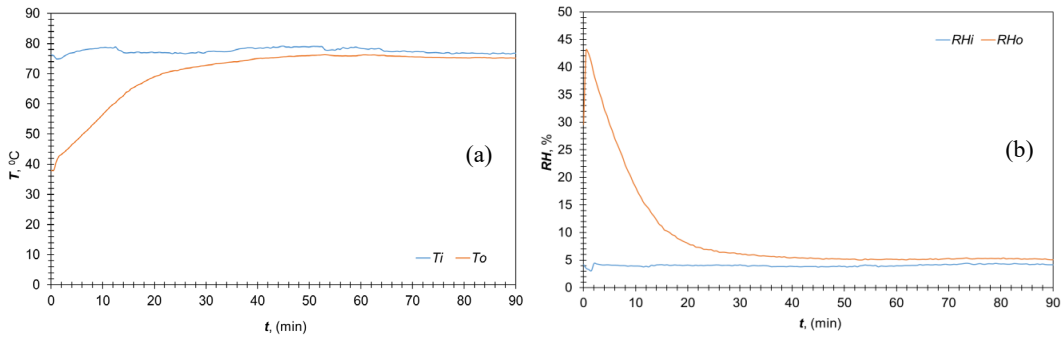

Figure 13. Temperature and (b) humidity variations during the charging process of CS-P/$CaCl_2$ at 2.1 m/s air velocity.

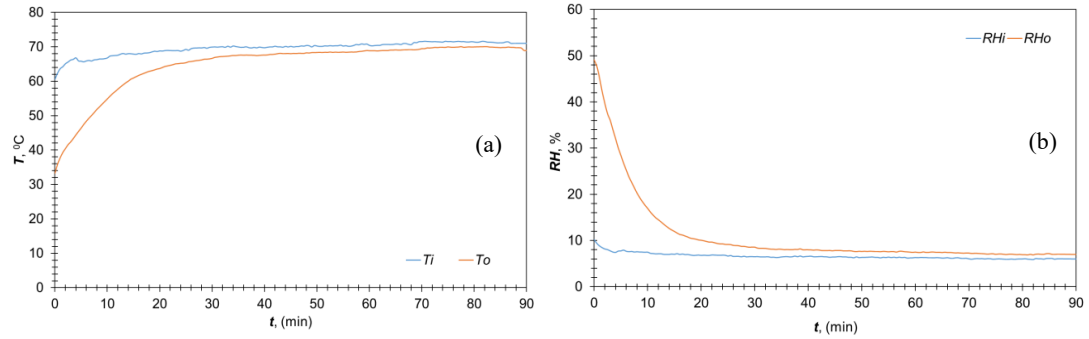

Figure 14. (a) Temperature and (b) humidity variations during the charging process of CS-P/$CaCl_2$ at

3.7 m/s air velocity.

3.3. Overall Cyclic Analysis

This section evaluates the cyclic charging–discharging performance of P/LiCl–$CaCl_2$, P/$CaCl_2$, and CS-P/$CaCl_2$ composite TCMs at different air velocities. Figure 15(a) presents their energy efficiencies. At 2.1 m/s, P/LiCl–$CaCl_2$ achieved 64%, increasing to 76.6% at 3.7 m/s. P/$CaCl_2$ showed lower efficiencies of 44.7% and 48.4%, respectively, while CS-P/$CaCl_2$ exhibited intermediate values of 64.2% and 72.2%. Energy efficiency increased with air velocity for all materials, with P/LiCl–$CaCl_2$ consistently outperforming the others. These results suggest that the presence of LiCl and smaller TCM particle size significantly enhance the thermal performance of TCMs, especially at higher air velocities, which is critical for improving the efficiency of TCES systems.

Exergy analysis was also conducted to assess the thermodynamic effectiveness of the system under varying airflow rates and TCM compositions. While energy analysis reveals how much heat is stored or released, exergy analysis offers insight into the quality of this energy and the degree of irreversibility present in the system processes. As shown in Figure 15(b), the P/LiCl–$CaCl_2$ composite outperformed both P/$CaCl_2$ and CS-P/$CaCl_2$ in terms of exergy efficiency. At an air velocity of 2.1 m/s, P/LiCl–$CaCl_2$ achieved an exergy efficiency of 10.5%, compared to 4.9% for P/$CaCl_2$ and 5.8% for CS-P/$CaCl_2$. At 3.7 m/s, the P/LiCl–$CaCl_2$ composite further improved to 11.2%, while P/$CaCl_2$ and CS-P/$CaCl_2$ remained much lower at 5.2% and 5.4%, respectively. Factors such as average charging temperature, temperature difference of air across the sorption bed, temperature lift during discharging, and ambient conditions significantly influence these results. The exergetic analysis indicates that at most 11.2% of the work potential invested during charging is recovered during discharging, highlighting a key limitation of TCES systems that warrants further investigation.

Although the investigations demonstrate relatively high cyclic energy efficiency (ranging from 44.7% to 76.6%), the cyclic exergy efficiency is much lower, between 4.9% and 11.2%. This difference is inherent to the definitions of these two metrics. Energy efficiency considers only the quantity of energy transferred, without regard to its usability or quality. In contrast, exergy efficiency evaluates how much of the input energy can be converted into useful work, considering ambient reference conditions and entropy generation. Since much of the recovered heat in TCES systems is low-grade and discharged near ambient temperature, its exergy content is inherently low. On the other hand, the charging process involves supplying thermal energy at relatively high temperatures exergy input during charging due to the higher quality of the supplied energy. This mismatch between high-grade input and low-grade output leads to increased exergy destruction and thus a lower overall exergy efficiency. Additionally, irreversible losses during adsorption/desorption cycles further degrade the exergy potential. As such, the lower exergy efficiency is not a sign of poor system design but rather reflects the real thermodynamic limitations of low-temperature TCES systems.

Figure 15(c) presents a comparison of the moisture absorbed and desorbed by the composite TCMs during the charging and discharging cycles. The P/LiCl–$CaCl_2$ composite material absorbed 394 g of moisture at an air velocity of 2.1 m/s and desorbed approximately 81.2% (320 g). When the air velocity increased to 3.7 m/s, the absorption amount reached 540 g, and 82.6% (446 g) of this was successfully recovered. This data demonstrates that increasing air velocity not only increased moisture retention capacity but also desorption efficiency. The P/$CaCl_2$ composite material absorbed 430 g of moisture at 2.1 m/s and desorbed 76.7% (330 g). At 3.7 m/s, 535 g was absorbed, and 78.5% (420 g) was released. On the other hand, the CS-P/$CaCl_2$ composite material absorbed 360 g of moisture at 2.1 m/s and desorbed 69.4% (250 g). At 3.7 m/s, 356 g was absorbed, but only 68.5% (244 g) was released. These results indicate that CS-P/$CaCl_2$ exhibited lower moisture cycling ability in comparison to P-$CaCl_2$, primarily due to the pumice particle size. The smaller particle size of the P-$CaCl_2$ (1-3 mm) increases the specific surface area, facilitating both moisture sorption and desorption. In contrast, the larger particle size (4–6 mm) in the CS-P/$CaCl_2$ limits the contact of TCM and the air as well as allows larger air passages, which reduces the convective heat and mass transfer. On the other hand, compared to the other two candidates, P/LiCl–$CaCl_2$ demonstrated superior moisture desorption performance, making it a more promising material for cyclic use, an essential factor in TCES applications.

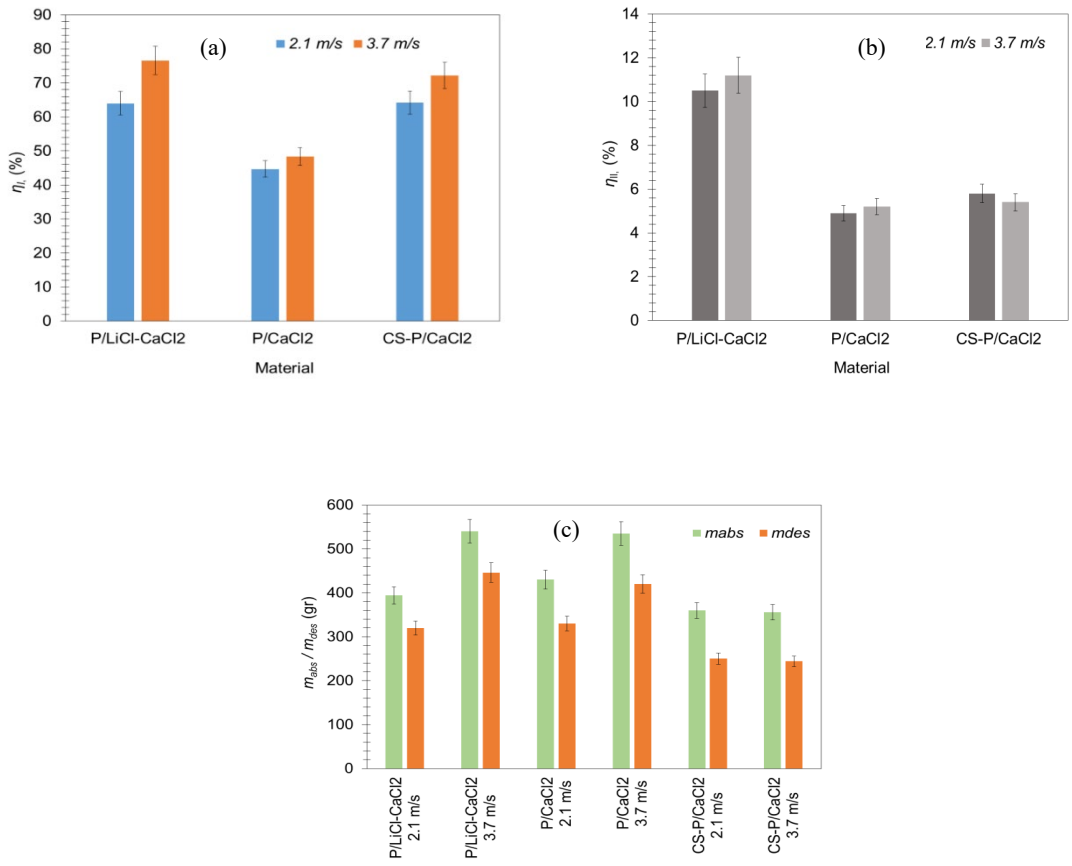

Figure 15. (a) Variations of energetic efficiency (b) exergetic efficiency (c) amount of moisture absorption/desorption under different air velocities.

As summarized in Table 1, P/LiCl–$CaCl_2$ consistently achieved the highest energy and exergy efficiencies, as well as the greatest energy storage density, across both tested air velocities. P/$CaCl_2$ ranked second in energy storage density but showed lower efficiencies, while CS-P/$CaCl_2$ displayed lowest moisture cycling ability and the lowest storage capacity. These trends highlight the influence of salt composition and pumice particle size on TCES performance.

The results obtained in this study, as detailed in Table 1, demonstrate the suitability of pumice-based salt-in-matrix composites for TCES applications. The cyclic efficiency and moisture sorption/desorption behavior of the materials closely align with previous findings reported in the literature (Abdullah Al Ghosini and Aydin, 2024). At a charging temperature of approximately 70 °C, about 70–80% of the absorbed moisture is desorbed, indicating strong potential for integration with solar thermal systems for residential heat storage. As shown in Table 1, the tested TCMs achieved energy storage densities of up to 181 kWh/m³ during a one-hour discharging operation, alongside energy efficiencies of up to 76.6% and exergy efficiencies of up to 11.2%. These values highlight the competitive performance of the P/LiCl–$CaCl_2$ composite in particular. The results obtained also indicate that performance could be further improved through optimization of operating parameters such as airflow rate and humidity. Future work should focus on refining TCM properties and assessing long-term cyclic stability. Additionally, encapsulation techniques may offer solutions to enhance heat and mass transfer, reduce pressure drop across the sorption bed, and mitigate agglomeration issues, key challenges in TCES systems.

Table 1. Summary of test results.

	P/LiCl–$CaCl_2$		*P/$CaCl_2$*		*CS-P/$CaCl_2$*	
	2.1 m/s	*3.7 m/s*	*2.1 m/s*	*3.7 m/s*	*2.1 m/s*	*3.7 m/s*
E_d *(kWh/m³)*	121.8	181.3	98	170.58	90.75	115.2
$\dot{Q}_o$ *(kW)*	0.43	0.63	0.34	0.60	0.32	0.40
$T_{o,p}$ *(^{0}C)*	46.4	47.7	42.5	39	40.9	39
$T_{i,chr}$ *(^{0}C)*	67.7	67.2	76.5	79.2	77.5	69.5
$T_{o,chr}$ *(^{0}C)*	57.6	60	62.8	66.8	70.4	65
$RH_{o,chr}$ *(%)*	16.3	13.8	12.6	10.4	8.9	10.8
$RH_{i,dc}$ *(%)*	63.7	63.5	68.3	68.4	73	75.4
m_{abs} *(gr)*	394	540	430	535	360	356
m_{des} *(gr)*	320	446	330	420	250	244
η_I *(%)*	64	76.6	44.7	48.4	64.2	72.2
η_{II} *(%)*	10.5	11.2	4.9	5.2	5.8	5.4

4. Conclusion

In this study, three different composite TCMs developed for TCES applications, P/LiCl–$CaCl_2$, P/$CaCl_2$ and CS-P/$CaCl_2$ were experimentally tested under laboratory conditions at different air velocities (2.1 m/s and 3.7 m/s). The following key conclusions were drawn from the experimental findings:

- Increasing air velocity significantly increased the E_d for all three TCMs. The P/LiCl–$CaCl_2$ composite exhibited the highest performance with an E_d value of 181.3 kWh/m³ at an air velocity of 3.7 m/s, compared to 170.5 kWh/m³ for P/$CaCl_2$ and 115.2 kWh/m³ for the CS-P/$CaCl_2$ composite at the same velocity. This indicates that the addition of LiCl increased the heat storage capacity.
- The exergetic efficiency of P/LiCl–$CaCl_2$ was measured as 10.5% at 2.1 m/s and 11.2% at 3.7 m/s. Under the same conditions, the efficiencies of P/$CaCl_2$ and CS-P/$CaCl_2$ were far lower, varying between 4.9% and 5.8%. This reflects reduced exergy destruction and a more effective utilization of the available work potential, attributable to the presence of LiCl in the P/LiCl–$CaCl_2$ composite.
- When evaluating moisture cycling performance, the P/LiCl–$CaCl_2$ composite TCM achieved the highest desorption rates—81.2% at 2.1 m/s and 82.6% at 3.7 m/s. The P/$CaCl_2$ composite showed intermediate performance, with 76.7% and 77.8% at the respective velocities. The lowest rate was recorded for CS-P/$CaCl_2$, at 69.4% and 68.5%. These results highlight the positive effect of smaller particle size in enhancing moisture desorption rates.
- Overall, the P/LiCl–$CaCl_2$ composite material demonstrated superior performance compared to P/$CaCl_2$ and CS-P/$CaCl_2$ in terms of energy density, exergetic efficiency and moisture cycling ability. The findings demonstrate that LiCl addition, particle size reduction, and increased air velocity are critical factors in improving the overall efficiency of TCES systems. These results provide important guidance for material selection and system design in TCES technologies.

Declaration of Competing Interest

The authors declare that they have no known competing financial interests or personal relationships that could have appeared to influence the work reported in this paper.

Funding and Acknowledgements

This work was supported by the Engineering and Physical Sciences Research Council [Horizon Europe Guarantee grant number: EP/Z002117/1].

Data Availability

Data will be made available on request.

References

Aarts, J., Fischer, H., Adan, O. and Huinink, H. (2025). Towards stable performance of salt hydrates in thermochemical energy storage: A review. *Journal of Energy Storage*, 114, p.115726. doi:https://doi.org/10.1016/j.est.2025.115726.

Abdullah Al Ghosini and Aydin, D. (2024). Comparative energy and exergy analyses of pumice and vermiculite-based salt-in-matrix composites for low-grade thermochemical heat storage applications. *International Journal of Exergy*, 43(3), pp.273–286. doi:https://doi.org/10.1504/ijex.2024.137565.

Abdullah, N., M. Koushaeian, Shah, N.A. and Chung, J.D. (2024). A review on thermochemical seasonal solar energy storage materials and modeling methods. *International Journal of Air-Conditioning and Refrigeration*, 32(1). doi:https://doi.org/10.1007/s44189-023-00044-6.

Barbosa, E. and Menon, A.K. (2024). Thermochemical energy storage using salt mixtures with improved hydration kinetics and cycling stability. *Journal of Energy Storage*, 90, pp.111916–111916. doi:https://doi.org/10.1016/j.est.2024.111916.

Buker, M.S., Mempouo, B. and Riffat, S.B. (2014). Performance evaluation and techno-economic analysis of a novel building integrated PV/T roof collector: An experimental validation. *Energy and Buildings*, 76, pp.164–175. doi:https://doi.org/10.1016/j.enbuild.2014.02.078.

Farcot, L., Le Pierrès, N. and Fourmigué, J.-F. (2019). Experimental investigation of a moving-bed heat storage thermochemical reactor with SrBr2/H2O couple. *Journal of Energy Storage*, 26, p.101009. doi:https://doi.org/10.1016/j.est.2019.101009.

Hao, C., Feng, G., Ma, C., Barreneche, C. and She, X. (2024). Performance analysis of a novel multi-module columnar packed bed reactor with salt hydrates for thermochemical heat storage. *Journal of Energy Storage*, 86, p.111170. doi:https://doi.org/10.1016/j.est.2024.111170.

Hu, Z., Luo, J., Jin, Y., Ke, F., Wang, W. and Yin, Q. (2025). Experimental study on thermochemical heat storage performance of expanded perlite-based SrCl2/CaCl2 binary hydrated salt composites. *Journal of Energy Storage*, 117, p.116199. doi:https://doi.org/10.1016/j.est.2025.116199.

Inada, A.A., Rezaei, M. and Aydin, D. (2025). Recent developments on open thermochemical energy storage towards decarbonised building space heating and cooling. *International Journal of Global Warming*, 35(2/3/4), pp.104–127. doi:https://doi.org/10.1504/ijgw.2025.145087.

John, M.K., Vishnu., K., Vishnu., C., Rohinikumar., B. and Muraleedharan, C. (2024). Experimental and numerical investigations on an open thermochemical energy storage system using low-temperature hydrate salt. *Thermal Science and Engineering Progress*, 53, p.102749. doi:https://doi.org/10.1016/j.tsep.2024.102749.

Karim Nejhad, M. and Aydin, D. (2019). Synthesize and hygro-thermal performance analysis of novel APC-CaCl2 composite sorbent for low-grade heat recovery, storage, and utilization. *Energy Sources, Part A: Recovery, Utilization, and Environmental Effects*, 43(23), pp.3011–3031. doi:https://doi.org/10.1080/15567036.2019.1666187.

Li, S., Wang, Y., Tang, X., Chang, Z. and Li, M. (2025). Hybrid nanoparticle and salt-modified aluminum fumarate metal-organic framework for thermochemical adsorption heat storage. *Chemical Engineering Journal*, pp.165801–165801. doi:https://doi.org/10.1016/j.cej.2025.165801.

Liu, X., Liu, X., Yang, F. and Wu, Y. (2024). Experimental investigation of low-temperature fluidised bed thermochemical energy storage with salt-mesoporous silica composite materials. *Applied energy*, 362, pp.122953–122953. doi:https://doi.org/10.1016/j.apenergy.2024.122953.

Mehrabadi, A. and Farid, M. (2018). New salt hydrate composite for low-grade thermal energy storage. *Energy*, 164, pp.194–203. doi:https://doi.org/10.1016/j.energy.2018.08.192.

Padamurthy, A., Gandla, P.K., Sheelwant, A., Vemanaboina, H., Paramasivam, P. and Ayanie, A.G. (2025). Emerging Trends and Future Prospects of Thermochemical Energy Storage Systems for Building Space and Water Heating Applications. *International Journal of Energy Research*, 2025(1). doi:https://doi.org/10.1155/er/6685290.

Wang, Y., Chen, T., Liu, S., Ji, W., Shen, Y., He, B., Li, Y. and Xu, Z. (2025). Development and system performance evaluation of new thermochemical energy storage composite materials for direct photothermal conversion at low temperature. *Energy*, 332, p.137161. doi:https://doi.org/10.1016/j.energy.2025.137161.

Wei, S., Zhou, W., Han, R., Gao, J., Zhao, G., Qin, Y. and Wang, C. (2022). Influence of minerals with different porous structures on thermochemical heat storage performance of $CaCl_2$-based composite sorbents. *Solar Energy Materials and Solar Cells*, 243, p.111769. doi:https://doi.org/10.1016/j.solmat.2022.111769.

Wei, W., Yang, L., Li, Y., Lu, G., Brookes, M., Huang, Y. and Fan, X. (2024). Experimental and simulation study of two-stage water adsorption in salt porous composites for advanced thermochemical heat storage. *Chemical Engineering Journal*, 482, p.149096. doi:https://doi.org/10.1016/j.cej.2024.149096.

Yu, N., Wang, R.Z., Lu, Z.S. and Wang, L.W. (2015). Study on consolidated composite sorbents impregnated with LiCl for thermal energy storage. *International Journal of Heat and Mass Transfer*, 84, pp.660–670. doi:https://doi.org/10.1016/j.ijheatmasstransfer.2015.01.065.

Zhang, Y., Chen, Z., Zhang, Y., Su, aY. and Riffat, S. (2024). Parameter control in synthesis of Vermiculite-CaCl2 composite materials for thermochemical adsorption heat storage. *Energy*, 291. doi:https://doi.org/10.1016/j.energy.2024.130478.

Zhang, Y., Chen, Z., Chen, J., Bottarelli, M., Su, Y. and Riffat, S. (2025). Experimental study on a thermochemical energy storage system for water heating with microchannel flat tube heat exchangers. *Energy*, 328, p.136539. doi:https://doi.org/10.1016/j.energy.2025.136539.